Inorg. Chem. **2008**, *47*, 7660−7672

Structural Variation within Homometallic Uranium(VI) Carboxyphosphonates: In Situ Ligand Synthesis, Directed Assembly, Metal−Ligand Coordination and Hydrogen Bonding

Karah E. Knope[†] and Christopher L. Cahill*[,†,‡]

Contribution from the Department of Chemistry, The George Washington University, 725 21st St. NW, Washington, D.C. 20052, and the Geophysical Laboratory, Carnegie Institution of Washington, 5251 Broad Branch Road NW, Washington, D.C. 20015

Received April 16, 2008

Four 2D uranium(VI) carboxyphosphonates, $(UO_2)(O_3PCH_2CO_2H)$ (**1**), $(UO_2)_4(HO_3PCH_2CO_2)(O_3PCH_2CO_2)_2(H_2O)_4 \cdot 3H_2O$ (**2**), $(UO_2)(O_3PCH_2CO_2) \cdot NH_4 \cdot H_2O$ (**3**), and $(UO_2)_3(O_3PCH(CH_3)CO_2)_2(O_3PCH(CH_3)CO_2H) \cdot 2NH_4 \cdot H_2O$ (**4**) have been prepared using hydrothermal techniques. Their crystal structures have been determined by single-crystal X-ray diffraction, and structural features have been confirmed by infrared spectroscopy. **1**, **2**, and **3** are constructed from the UO_2^{2+} cation and phosphonoacetate, $(O_3PCH_2CO_2)$, molecules, whereas **4** consists of U(VI) coordinated to 2-phosphonopropionate, $(O_3PCH(CH_3)CO_2)$, units. The thermal and fluorescent behaviors of these materials have also been investigated. The organophosphonate linkers observed in **2** and **4** were produced via the in situ hydrolysis of trialkylphosphonate starting materials.

Introduction

Within the field of inorganic materials chemistry, research efforts into the synthesis and design of extended, open-framework materials with interesting physiochemical properties have exploded.[1−14] Metal phosphonate chemistry, in particular, has attracted much attention due to the diversity with which these materials assemble into a vast range of structure types.[1,3,15−18] Additionally, these compounds exhibit promising features that may potentially be applied to areas such as catalysis, ion exchange, sensor technology, and magnetics.[19] To this end, researchers have explored the synthesis and properties of phosphonate-containing structures utilizing a range of metal centers,[20−25] templates,[23,25,26] and phosphonate ligands.[16,27−30] From a structural perspective and in the context

[†] The George Washington University.
[‡] Carnegie Institution of Washington.

(1) Cheetham, A. K.; Ferey, G.; Loiseau, T. *Angew. Chem., Int. Ed.* **1999**, *38*, 3268–3292.
(2) Cahill, C. L.; de Lill, D. T.; Frisch, M. *Cryst. Eng. Commun.* **2007**, *9*, 15–26.
(3) Clearfield, A. *Chem. Mater.* **1998**, *10*, 2801–2810.
(4) Rao, C. N. R.; Natarajan, S.; Vaidhyanathan, R. *Angew. Chem., Int. Ed.* **2004**, *43*, 1466–1496.
(5) Yaghi, O. M.; Li, H.; Davis, C.; Richardson, D.; Groy, T. L. *Acc. Chem. Res.* **1998**, *31*, 474–484.
(6) Uemura, K.; Matsuda, R.; Kitagawa, S. *J. Solid State Chem.* **2005**, *178*, 2420–2429.
(7) Eddaoudi, M.; Moler, D. B.; Li, H.; Chen, B.; Reineke, T. M.; O'Keeffe, M.; Yaghi, O. M. *Acc. Chem. Res.* **2001**, *34*, 319–330.
(8) Hill, R. J.; Long, D.-L.; Hubberstey, P.; Schroder, M.; Champness, N. R. *J. Solid State Chem.* **2005**, *178*, 2414–2419.
(9) Janiak, C. *Dalton Trans.* **2003**, 2781–2804.
(10) Kitagawa, S.; Kitaura, R.; Noro, S-i. *Angew. Chem., Int. Ed.* **2004**, *43*, 2334–2375.
(11) Kepert, C. J. *Chem. Commun. (Cambridge, United Kingdom)* **2006**, 695–700.
(12) Férey, G. *Chem. Mater.* **2001**, *13*, 3084–3098.
(13) Rosi, N. L.; Eddaoudi, M.; Kim, J.; O'Keeffe, M.; Yaghi, O. M. *Cryst. Eng. Comm.* **2002**, *4*, 401–404.
(14) Kitagawa, S.; Matsuda, R. *Coord. Chem. Rev.* **2007**, *251*, 2490–2509.
(15) Clearfield, A. *J. Alloys Compd.* **2006**, *418*, 128–138.
(16) Maeda, K. *Microporous Mesoporous Mater.* **2004**, *73*, 47–55.
(17) Clearfield, A. *Curr. Opinion Solid State Mater. Sci.* **1996**, *1*, 268–278.
(18) Clearfield, A. *Curr. Opin. Solid State Mater. Sci.* **2002**, *6*, 495–506.
(19) Clearfield, A. In *Prog. Inorg. Chem.*; Karlin, K. D., Ed.; John Wiley & Sons: New York, 1998; Vol. *47*, pp 371−510.
(20) Bray, T. H.; Nelson, A. G. D.; Jin, G. B.; Haire, R. G.; Albrecht-Schmitt, T. E. *Inorg. Chem.* **2007**, *46*, 10959–10961.
(21) Dines, M. B.; Griffith, P. C. *Polyhedron* **1983**, *2*, 607–611.
(22) Harrison, W. T. A.; Dussack, L. L.; Jacobson, A. J. *Inorg. Chem.* **1996**, *35*, 1461–1467.
(23) Doran, M. B.; Norquist, A. J.; O'Hare, D. *Chem. Mater.* **2003**, *15*, 1449–1455.
(24) Poojary, D. M.; Zhang, B.; Clearfield, A. *J. Am. Chem. Soc.* **1997**, *119*, 12550–12559.
(25) Zhang, X. M.; Hou, J. J.; Zhang, W. X.; Chen, X. M. *Inorg. Chem.* **2006**, *45*, 8120–8125.
(26) Zhu, J.; Bu, X.; Feng, P.; Stucky, G. D. *J. Am. Chem. Soc.* **2000**, *122*, 11563–11564.
(27) Mao, J.-G.; Clearfield, A. *Inorg. Chem.* **2002**, *41*, 2319–2324.
(28) Ying, S.-M.; Mao, J.-G. *Cryst. Growth Des.* **2006**, *6*, 964–968.

10.1021/ic800683m CCC: $40.75
Published on Web 07/31/2008

Scheme 1. The Three Carboxyphosphonate Ligands Used in This Study: Phosphonoacetic Acid (ppa), Triethylphosphonoacetate (teppa), and Triethyl 2-Phoshonopropionate (te-2-pp)[a]

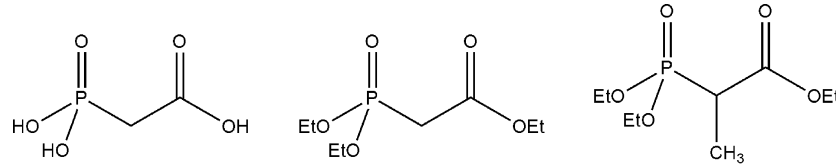

[a] Note: * denotes ligands that undergo in situ ester hydrolysis.

Scheme 2. Hydrolysis Scheme for Triakylester Carboxyphosphonates

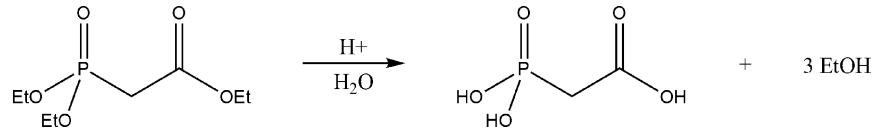

of preparing new phosphonate materials, researchers have surveyed mono-, di-,[31] amino-, sulfonate-,[32,33] and carboxyphosphonates[29] in combination with group II,[34] transition,[24,26,35–37] and lanthanide[29,33,38–41] metal ions.

Actinide phosphonates, despite their relevance to nuclear waste stewardship and separation processes, have been less thoroughly examined.[20,42–44] The first well characterized neptunium(IV) methylphosphonate was just recently reported,[20] and few thorium(IV) phosphonates have been detailed.[21] The synthesis, solid-state structures, and physical properties of uranium(VI) phosphonates have most frequently been described.[23,45–49]

These materials adopt linear-chain, layered, and tubular architectures. Moreover, a number of interesting properties have been observed. For example, within a uranyl phenylphosphonate system, Clearfield et al. reported the room-temperature transformation of a nonluminescent cis (α-UPP) into a strongly luminescent trans (*β*-UPP).[45] Subsequent exposure of the two linear-chain structures, (α-UPP) and (*β*-UPP), to sodium or calcium ions resulted in a tubular phase, (*γ*-UPP).[46]

The architectures of the U(VI) phosphonate materials reported thus far, including those mentioned above, have each been assembled via monofunctional linkers. Alternatively and often with the intent of promoting increased dimensionality or conveying specific properties to a product, researchers have used bifunctional organic species to synthesize new compounds and topologies. Within hexavalent uranium systems specifically, efforts to prepare and structurally characterize UO_2^{2+} containing extended structures using dicarboxylate linkers have been quite successful.[2,50–61] Inspired by the fruitfulness of these systems and given the rich structural variety and interesting properties observed for the few uranium(VI) monophosphonate compounds reported, we explored hydrothermal reactions of UO_2^{2+} with the carboxyphosphonate ligands depicted in Scheme 1. From a structural perspective, carboxyphosphonates are attractive candidates for U(VI) inorganic−organic materials synthesis and, unlike the organophosphonates previously used to construct uranium(VI) solid-state assemblies, they impart bi- and/or heterofunctionallity. The bifunctional nature is of interest as it has the propensity to promote the formation of network structures, whereas the heterofunctionality allows us to consider the affinity of the UO_2^{2+} cation for carboxy and/or phosphonate oxygen atoms as well as metal−organic

(29) Tang, S.-F.; Song, J.-L.; Mao, J.-G. *Eur. J. Inorg. Chem.* **2006**, *2006*, 2011–2019.
(30) Serre, C.; Ferey, G. *Inorg. Chem.* **2001**, *40*, 5350–5353.
(31) Gomez-Alcantara, M. M.; Cabeza, A.; Martinez-Lara, M.; Aranda, M. A. G.; Suau, R.; Bhuvanesh, N.; Clearfield, A. *Inorg. Chem.* **2004**, *43*, 5283–5293.
(32) Song, J.-L.; Lei, C.; Mao, J.-G. *Inorg. Chem.* **2004**, *43*, 5630–5634.
(33) Du, Z. Y.; Xu, H. B.; Mao, J.-G. *Inorg. Chem.* **2006**, *45*, 9780–9788.
(34) Svoboda, J.; Zima, V.; Benes, L.; Melanova, K.; Vlcek, M. *Inorg. Chem.* **2005**, *44*, 9968–9976.
(35) Hou, J.-J.; Zhang, X.-M. *Cryst. Growth Des.* **2006**, *6*, 1445–1452.
(36) Chen, Z.; Weng, L.; Zhao, D. *Inorg. Chem. Commun.* **2007**, *10*, 447–450.
(37) Bonavia, G.; Haushalter, R. C.; O'Connor, C. J.; Zubieta, J. *Inorg. Chem.* **1996**, *35*, 5603–5612.
(38) Mao, J.-G. *Coord. Chem. Rev.* **2007**, *251*, 1493–1520.
(39) Serre, C.; Stock, N.; Bein, T.; Ferey, G. *Inorg. Chem.* **2004**, *43*, 3159–3163.
(40) Tang, Si-Fu.; Song, J.-L.; Mao, J.-G. *Cryst. Growth Des.* **2006**, *6*, 2322–2326.
(41) Huang, Y.-L.; Huang, M.-Y.; Chan, T.-H.; Chang, B.-C.; Lii, K.-H. *Chem. Mater.* **2007**, *19*, 3232–3237.
(42) Nash, K. L. *J. Alloys Compd.* **1997**, *249*, 33–40.
(43) Jensen, M. P.; Beitz, J. V.; Rogers, R. D.; Nash, K. L. *J. Chem. Soc., Dalton Trans.* **2000**, *18*, 3058–3064.
(44) Chiariza, R.; Horwitz, E. P.; Alexandrators, S. D.; Gula, M. J. *Sep. Sci. Technol.* **1997**, *32*, 1–35.
(45) Grohol, D.; Clearfield, A. *J. Am. Chem. Soc.* **1997**, *119*, 4662–4668.
(46) Grohol, D.; Clearfield, A. *J. Am. Chem. Soc.* **1997**, *119*, 9301–9302.
(47) Grohol, D.; Gingl, F.; Clearfield, A. *Inorg. Chem.* **1999**, *38*, 751–756.
(48) Grohol, D.; Subramanian, M. A.; Poojary, D. M.; Clearfield, A. *Inorg. Chem.* **1996**, *35*, 5264–5271.
(49) Bao, S.-S.; Chen, G.-S.; Wang, Y.; Li, Y.-Z.; Zheng, L.-M.; Luo, Q.-H. *Inorg. Chem.* **2006**, *45*, 1124–1129.
(50) Kim, J.-Y.; Norquist, A. J.; O'Hare, D. *Dalton Trans.* **2003**, 2813–2814.
(51) Borkowski, L. A.; Cahill, C. L. *Cryst. Growth Des.* **2006**, *6*, 2241–2247.
(52) Borkowski, L. A.; Cahill, C. L. *Cryst. Growth Des.* **2006**, *6*, 2248–2259.
(53) Frisch, M.; Cahill, C. L. *Dalton Trans.* **2005**, 1518–1523.
(54) Frisch, M.; Cahill, C. L. *Dalton Trans.* **2006**, 4679–4690.
(55) Thuery, P. *Chem. Commun.* **2006**, 853–855.
(56) Thuery, P. *Inorg. Chem.* **2007**, *46*, 2307–2315.
(57) Thuery, P. *Polyhedron* **2007**, *26*, 101–106.
(58) Jiang, Y.-S.; Yu, Z.-T.; Liao, Z.-L.; Li, G.-H.; Chen, J.-S. *Polyhedron* **2006**, *25*, 1359–1366.
(59) Chen, W.; Yuan, H.-M.; Wang, J.-Y.; Liu, Z.-Y.; Xu, J.-J.; Yang, M.; Chen, J.-S. *J. Am. Chem. Soc.* **2003**, *125*, 9266–9267.
(60) Zheng, Y.-Z.; Tong, M.-L.; Chen, X.-M. *Eur. J. Inorg. Chem.* **2005**, *410*, 9–4117.
(61) Duvieubourg, L.; Nowogrocki, G.; Abraham, F.; Grandjean, S. *J. Solid State Chem.* **2005**, *178*, 3437–3444.

Table 1. Synthetic Details for **1**−**4**

	1	2	3	4
$(UO_2)(NO_3)_2 \cdot 6H_2O$	0.175 g (0.35mmol)	0.175 g (0.35mmol)		
$(UO_2)(CH_3CO_2)_2 \cdot 2H_2O$			0.150 g (0.35 mmol)	0.148 g (0.35 mmol)
ligand[a]	ppa	teppa	teppa	te-2-pp
	0.098 g	0.070 mL	0.155 mL	0.155 mL
	(0.70 mmol)	(0.35 mmol)	(0.76 mmol)	(0.70 mmol)
NH_4Cl			0.094 g	0.096 g
			(1.76 mmol)	(1.8 mmol)
H_2O	4 g	4 g	4 g	4 g
	(224 mmol)	(224 mmol)	(224 mmol)	(224 mmol)
molar ratios	1:2:640	1:1:640	1:2:5:640	1:2:5:640
time (d)	3	3	5	5
cryst description	plate	needle	plate	plate
yield (%) based on uranium	50	75	85	90
EA[b] Observed (Calcd)	C 6.00% (5.89%)	C 4.37% (4.45%)	C 5.42% (5.42%)	C 8.43% (8.20%)
	H 0.77% (0.74%)	H 1.34% (1.31%)	N 3.06% (3.16%)	N 2.11% (2.13%)
			H 1.62% (1.82%)	H 1.85% (1.76%)

[a] Phosphonoacetic acid (ppa); triethylphosphonoacetate (teppa); triethyl 2-phosphonopropionate (te-2-pp). [b] Elemental analysis (*EA*), Galbraith Laboratories, Knoxville, TN.

coordination modes that may contribute to the assembly and stabilization of the crystalline products.

The most common synthetic approach for obtaining new materials is typically via the direct reaction of a metal salt with a linker that will ultimately be observed in the solid-state structure. Alternatively and more recently, in situ ligand formation has demonstrated usefulness synthetically.[62] This route has been hailed as a new approach to crystal engineering with some of the most notable (potential) benefits including enhanced single-crystal growth, simplified syntheses, greener routes to materials, and the preparation of compounds not accessible otherwise (directly).[62–67] With regard to synthetic inorganic chemistry, the stability and insolubility of metal phosphonates, in particular, has made it historically difficult to isolate crystals suitable for characterization by X-ray diffraction. Researchers have since employed in situ ester hydrolysis reactions, such as that illustrated in Scheme 2, to promote the formation and growth of single crystals.[35,68] In an attempt to address the value of such in situ reactions in these systems, we examined the syntheses of uranyl carboxyphosphonates via direct and in situ ligand formation assembly pathways.

Reported herein are the syntheses, crystal structures, and thermal and fluorescent behavior of four U(VI) carboxyphosphonates, $(UO_2)(O_3PCH_2CO_2H)$ (**1**), $(UO_2)_4(HO_3PCH_2CO_2)(O_3PCH_2CO_2)_2(H_2O)_4 \cdot 3H_2O$ (**2**), $(UO_2)(O_3PCH_2CO_2) \cdot NH_4 \cdot H_2O$ (**3**), and $(UO_2)_3(O_3PCH(CH_3)CO_2)_2(O_3PCH(CH_3)CO_2H) \cdot 2NH_4 \cdot H_2O$ (**4**). To the best of our knowledge, previous reports of crystalline uranyl phosphonate materials have predominately been limited to those containing monophosphonates.[19,23,45,46] The compounds presented here further augment the already abundant structural chemistry of uranyl bearing extended networks and represent the first examples of uranium(VI) carboxyphosphonates. In situ ligand formation and the influence of the spectator species on product formation are also discussed. Moreover, structural features that contribute to the assembly and stabilization of the crystalline materials are examined.

Experimental Section

Synthesis. Caution! *Whereas the uranium oxyacetate* $(UO_2)(CH_3COO)_2 \cdot 2H_2O$ *and the uranium oxynitrate* $(UO_2)(NO_3)_2 \cdot 6H_2O$ *used in this investigation contain depleted uranium, standard precautions for handling radioactive substances should be followed.*

1−**4** were synthesized hydrothermally as outlined in Table 1. The reactants were placed into a 23 mL Teflon-lined Parr bomb that was then sealed and heated statically at 150 °C for 3 or 5 days. Upon cooling to room temperature, the mother liquor was decanted and yellow crystals were obtained. The crystals were washed with distilled water, sonicated in ethanol, washed in ethanol, and then allowed to air-dry at room temperature.

X-ray Structure Determination. A single crystal from each of the samples was isolated from the bulk and mounted on a glass fiber. Reflections were collected at room temperature using a Bruker SMART diffractometer equipped with an APEX II CCD detector using Mo Kα radiation and a combination of 0.5° ω and φ scans. The data were integrated with the *SAINT* software package.[69] The data were corrected for absorption using *SADABS*.[70] All compounds were solved using direct methods and refined using *SHELXL-97*[71] within the *WinGX* software suite.[72] Satisfactory refinements as well as tests for missing symmetry, using *Platon*,[73] indicated that no obvious space group changes were needed or suggested. Crystallographic data for **1**−**4** are provided in Table 2.

All non-hydrogen atoms were located using difference Fourier maps and ultimately all non-hydrogen atoms were refined anisotropically. Hydrogen atoms residing on the carbon atoms of the phosphonocarboxylate ligand in all of the structures were placed in calculated positions and bond distances were fixed at 0.97 Å.

(62) Zhang, X.-M. *Coord. Chem. Rev.* **2005**, *249*, 1201–1219.
(63) Chen, X. M.; Tong, M. L. *Acc. Chem. Res.* **2007**, *40*, 162–170.
(64) Knope, K. E.; Cahill, C. L. *Inorg. Chem.* **2007**, *46*, 6607–6612.
(65) Han, L.; Bu, X.; Zhang, Q.; Feng, P. *Inorg. Chem.* **2006**, *45*, 5736–5738.
(66) Hu, X.-X.; Xu, J.-Q.; Cheng, P.; Chen, X.-Y.; Cui, X.-B.; Song, J.-F.; Yang, G.-D.; Wang, T.-G. *Inorg. Chem.* **2004**, *43*, 2261–2266.
(67) Li, X.; Cao, R.; sun, D.; Shi, Q.; Bi, W.; Hong, M. *Inorg. Chem. Commun.* **2003**, *6*, 815–818.
(68) Hix, G. B.; Turner, A.; Kariuki, B. M.; Tremayne, M.; MacLean, E. J. *J. Mater. Chem.* **2002**, *12*, 3220–3227.
(69) *SAINT Area-Detector Integration Software*; Siemens Industrial Automation, Inc.: Madison, WI, 1998.
(70) Sheldrick, G. M. *SADABS, v. 2.03*, University of Göttingen: Göttingen, Germany, 2002.
(71) Sheldrick, G. M. *Acta Crystallogr.* **2008**, *A64*, 112–122.
(72) Farrugia, L. J. *J. Appl. Crystallogr.* **1999**, *32*, 837–838.
(73) Spek, A. L. *Acta Crystallogr., Sect. A* **1990**, *46*, C34.

Table 2. Crystallographic Data and Structure Refinement for **1**−**4**

	1	**2**	**3**	**4**
empirical formula	$C_2H_3O_7PU$	$C_6H_{21}O_{30}P_3U_3$	$C_2H_8NO_8PU$	$C_9H_{25}N_2O_{23}P_3U_3$
fw	408.04	1618.25	443.09	1336.31
temp (K)	295(2)	295(2)	295(2)	295(2)
λ (Mo Kα)	0.71073	0.71073	0.71073	0.71073
system	monoclinic	triclinic	orthorhombic	monoclinic
space group	$P2_1/c$	$P\bar{1}$	$Pbca$	$P2_1/m$
a (Å)	6.6927(10)	6.3474(4)	9.5896(4)	8.7542(6)
b (Å)	7.1348(11)	15.5483(10)	13.3487(6)	17.8712(12)
c (Å)	14.307(2)	15.7309(10)	13.4502(6)	9.0548(6)
α (°)	90	97.3360(10)	90	90
β (°)	103.015(2)	91.5810(10)	90	104.2950(10)
γ (°)	90	90.8890(10)	90	90
V (Å^3)	665.61(18)	1538.92(17)	1721.74(13)	1372.74(16)
Z	4	2	8	2
D_{calcd} (g·cm^{-3})	4.072	3.492	3.419	3.233
μ (mm^{-1})	24.616	21.247	19.059	17.926
$R_1{}^a$ [$I > 2\sigma(I)$]	0.0195	0.0428	0.0196	0.0281
$wR_2{}^a$	0.0442	0.0985	0.0354	0.0405

^{a} $R_1 = \Sigma||F_o| - |F_c||/\Sigma|F_o|$; $wR_2 = \{\Sigma[w(F_o^2 - F_c^2)^2/\Sigma[w(F_o^2)^2]\}^{1/2}$.

Structure **1** contains a $-CO_2H$ group of which the hydrogen atom was located in the difference Fourier map and freely refined. Similarly, during the refinement of **3**, hydrogen atoms of the solvent water and ammonium molecules were located in the difference Fourier maps, and the hydrogens were freely refined with distance restraints of 0.80 and 0.89 Å, respectively.

The hydrogen atoms of the bound water molecules were not located in the difference Fourier map of **2** during refinement. The structure also contains disordered solvent water. Four solvent water molecules were located in the difference Fourier map, of which two were modeled at 50% occupancy resulting in three unbound water molecules per formula unit. Using *Squeeze*[74] within the *PLATON* software package, the total solvent accessible void volume and electron count per cell were found to be 287.5 Å^3 and 83, respectively. As $Z = 2$, these results are consistent with 4 water molecules per formula unit. Alternatively, the initial weight loss of approximately 3% observed in the TGA of **2** is consistent with a loss of 3 water molecules. Elemental analysis observed (Calcd): 4 solvent water molecules: C 4.40% (4.45%); H 1.42% (1.31%). Three solvent water molecules: C 4.37% (4.45%); H 1.34% (1.31%). These results are admittedly inconclusive yet for discussion purposes; the results presented herein will reflect the structure as modeled with 3 water molecules.

Structure **4** contains a 2-phosphonopropionate unit that is disordered across a mirror plane. As such, the carboxylate and methyl groups of this molecule were modeled at 50% occupancy. Hydrogen atoms of the solvent water and ammonium molecules were not located in the difference Fourier map. In addition to charge balance requirements, the presence of NH_4^+ in **4** is consistent with the carbon, hydrogen, and nitrogen analysis and the stretch observed at 1418 cm-1 in the IR spectrum (SI17 in the Supporting Information) of **4**.

Powder X-ray diffraction data were collected for **1**−**4** using a Rigaku Miniflex diffractometer (Cu Kα, 3−60°) and manipulated using the *JADE* software package.[75] As shown in SI1−4 in the Supporting Information, agreement between the calculated and observed patterns confirmed phase purity for the bulk sample.

Characterization. Thermogravimetric analysis (TGA) was performed on a PerkinElmer Pyris1 at a rate of 5 °C/min over a temperature range of 30−600 °C under flowing nitrogen gas. IR spectra were obtained on a PerkinElmer Spectrum RX1 FTIR system. The sample was diluted with spectroscopic KBr and pressed into a pellet. Scans were run over the range 4000−400 cm^{-1} with 8 scans and 2 cm^{-1} resolution. Fluorescent studies were conducted on a Shimadzu RF-5301 PC Spectrofluorophotometer (uranium excitation wavelength: 365 nm;[76] emission wavelength: 400−600 nm; slit width: 1.5 (excitation) and 1.5 (emission); sensitivity: high with a UV-35 filter).

Results

Structure Description. The crystal structures of **1**−**4** all consist of pentagonal bipyramid polyhedra constructed from the uranyl cation (UO_2^{2+}) equatorially coordinated to five oxygen atoms. Within these compounds, a central uranium(VI) atom is bound to two axial oxygen atoms with an average $U-O_{ur}$ distance of 1.76 Å and an average $O_{ur}-U-O_{ur}$ bond angle of 178.5°. Table 3 lists selected bond lengths and angles for **1**−**4**. Even though **1**−**4** are assembled from similar building units, significant topological diversity is observed and will be discussed. *ORTEP* illustrations for **1**−**4** are included in the Supporting Information (Figures SI5, SI6, SI8 and SI9).

The structure of **1**, $(UO_2)(O_3PCH_2CO_2H)$, consists of chains of edge-shared pentagonal bipyramids that propagate along [010]. Illustrated in part a of Figure 1, these chains are linked by phosphonate oxygen atoms to form uranophane type sheets,[77,78] resulting in an overall 2D structure. The pentagonal bipyramids each consist of the near linear UO_2^{2+} cation equatorially coordinated to five phosphonate oxygens (part b of Figure 1) from four phosphonoacetate molecules. The structure contains one crystallographically unique uranium metal center that is

(74) van der Sluis, P.; Spek, A. L. *Acta Crystallogr., Sect. A* **1990**, *46*, 194–201.
(75) *JADE; V6.1*; Materials Data Inc.: Livermore, CA.
(76) Almond, P. M.; Talley, C. E.; Bean, A. C.; Peper, S. M.; Albrecht-Schmitt, T. E. *J. Solid State Chem.* **2000**, *154*, 635–641.
(77) Burns P. C. In *Structural Chemistry of Inorganic Actinide Compounds*; Krivovichev, S. V., Burns, P. C., Tananaev, I. G., Eds.; Elsevier: Oxford, 2007; pp 1−30.
(78) Locock, A. J. In *Structural Chemistry of Inorganic Actinide Compounds*; Krivovichev, S. V., Burns, P. C., Tananaev, I. G., Eds.; Elsevier: Oxford, 2007, pp 217−278.

Table 3. Selected Bond Lengths (Angstroms) and Angles (Degrees) for **1**−**4**

		1[a]	
U(1)−O(4)	1.757(3)	C(1)−C(2)	1.522(6)
U(1)−O(2)	1.760(3)	O(6)−C(2)	1.302(5)
U(1)−O(3)	2.293(3)	O(7)−C(2)	1.209(5)
U(1)−O(1)	2.380(2)	O(6)H···O(7)	2.658(5)
U(1)−O(5)	2.405(3)	O(4)−U(1)−O(2)	177.2(1)
O(3)−P(1)	1.503(3)		
P(1)−O(5)[1]	1.538(3)		
P(1)−C(1)	1.801(4)		
		2	
U(1)−O(4)	1.756(9)	P(2)−O(1)	1.492(8)
U(1)−O(5)	1.764(9)	P(1)−C(1)	1.807(13)
U(2)−O(15)	1.738(9)	C(1)−C(2)	1.53(2)
U(2)−O(16)	1.752(9)	C(3)−C(4)	1.499(16)
U(3)−O(20)	1.721(10)	O(2)−C(2)	1.271(15)
U(3)−O(21)	1.765(10)	O(4)−U(1)−O(5)	179.5(4)
U(4)−O(22)	1.777(10)	O(15)−U(2)−O(16)	178.1(4)
U(4)−O(23)	1.757(10)	O(20)−U(3)−O(21)	177.6(4)
		O(23)−U(4)−O(22)	179.0(6)
		3	
U(1)−O(7)	1.769(3)	O(5)−C(2)[1]	1.259(4)
U(1)−O(6)	1.777(3)	C(1)−C(2)	1.522(5)
U(1)−O(1)	2.348(3)	O(10)−H(10A)···O(7)	2.990(5)
O(1)−P(1)	1.515(3)	O(10)−H(10B)···O(1)	2.819(5)
C(1)−P(1)	1.812(4)	N(20)−H(23)···O(10)	2.799(6)
O(2)−C(2)	1.253(5)	O(7)−U(1)−O(6)	179.8(1)
		4	
U(1)−O(8)	1.763(5)	P(1)−C(4)	1.824(8)
U(1)−O(4)	1.773(5)	P(2)−C(2)	1.826(6)
U(1)−O(1)	2.518(3)	C(1)−C(2)	1.495(7)
U(2)−O(5)	1.760(4)	C(4)−C(5)	1.511(9)
U(2)−O(9)	1.771(4)	O(8)−U(1)−O(4)	178.2(3)
U(2)−O(6)	2.474(3)	O(5)−U(2)−O(9)	178.6(1)
O(1)−C(1)	1.287(6)	C(3A)-H(3A)···O(5)	3.278(11)
O(2)−P(2)	1.517(4)	C(3B)-H(3B)···O(5)	3.480(15)
O(3)−P(1)	1.523(5)	C(3B)-H(3B)···O(41)	2.754(18)
O(6)−C(1)	1.265(6)		

[a] Symmetry transformations: (**1**) 1, $-x+1$, $y-{}^1/_2$, $-z+{}^1/_2$; (**3**) 1, $x+{}^1/_2$, $-y+{}^1/_2$, $-z+1$.

bound to two axial O atoms (O2 and O4) at a distance of 1.760 (3) and 1.757 (3) Å respectively with a O2−U1−O4 bond angle of 177.2 (1)°. The phosphonoacetate ligand displays two distinct modes of connectivity to each U(VI) metal center. Three phosphonoacetate units are bound in a monodentate fashion through a phosphonate oxygen (O1, O3, O5) with an average bond distance of 2.359 Å, whereas the fourth phosphonoacetate ligand is bound in a bidentate manner through phosphonate oxygens, O1 and O5, at an average bond distance of 2.522 Å. Depicted in part a of Figure 2, the carboxylate oxygens (O6 and O7) of the phosphonoacetate molecules extend into the interlayer where, as illustrated in part b of Figure 2, head-to-head O(6), O(7) hydrogen bonding (O6···O7, O6−H···O7: 2.658(5) Å, 161.0 °), adds to the stabilization of the structure.

The structure of **2**, $(UO_2)_4(HO_3PCH_2CO_2)(O_3PCH_2CO_2)_2(H_2O)_4\cdot 3H_2O$, contains point-shared $(UO_2)_2O_9$ dimers (Figure 3) linked via one distinct phosphonoacetate molecule to form chains that extend infinitely along [100]. The chains are connected to discrete $U(3)O_2^{2+}$ pentagonal bipyramids down [001] through two additional phosphonoacetate units to result in the 2D sheets shown in Figure 3. Illustrated in Figure 4, phosphonate tetrahedra link successive sheets via coordination to isolated $U(4)O_2^{2+}$ pentagonal bipyramids to form thick slabs that stack along [010]. The structure is built from four unique uranium metal centers where each site is characteristically bound to two axial oxygen atoms (O4, O5, O15, O16, O20−O23), to form the UO_2^{2+} cation, with an average U−O bond distance of 1.751 Å and an average O−U−O bond angle of 178.4°. Additionally, each UO_2^{2+} is equatorially bound to five oxygen atoms to result in pentagonal bipyramid geometry. U(1) is coordinated to three phosphonoacetate units, two of which are bound in a bidentate fashion through both a phosphonate oxygen (O3, O9) and a carboxylate oxygen (O2, O11) with average bond distances of 2.341 and 2.454 Å, respectively. The coordination sphere of U1 is completed by an additional phosphonate oxygen (O1) from a third phosphonoacetate molecule that is further coordinated to U(2) in a bidentate fashion via carboxylate oxygens O11 and O12. U(2) is additionally bound to two phosphonate oxygens (O10, O14) and one carboxylate oxygen (O13) from three phosphonoacetate molecules that exhibit monodentate modes of connectivity. Coordination of O11 to both U(1) and U(2) results in point-shared $(UO_2)_2O_9$ dimers that are connected to subsequent dimers via a single phosphonacetate unit. The coordination sphere of U(3) is constructed from the uranyl cation equatorially bound to a water molecule (O19), one bidentate, and two monodentate phosphonoacetate molecules. The bidentate ligand is connected through a phosphonate oxygen (O18) and a carboxylate oxygen (O13). The two monodentate units, which exhibit different binding modes, are either bound via a carboxylate oxygen (O8) or a phosphonate oxygen (O7). Like the metal centers that compose the sheet, U(4) is also constructed from UO_2^{2+} coordinated to five oxygen atoms to form a pentagonal bipyramid geometry. The metal center is equatorially bound to three water molecules (O24, O25, and O27)[79] and two phosphonate oxygens (O6 and O26) at average bond distances of 2.502 and 2.285 Å, respectively. Solvent water resides in the interlayer as well as in the channels of the slabs.

The structure of **3**, $(UO_2)(O_3PCH_2CO_2)\cdot NH_4\cdot H_2O$, consists of one crystallographically unique uranium metal center that is bound to two axial oxygen atoms (O6 and O7) at a distance of 1.777(3) and 1.769(3) Å, respectively, to form a near linear UO_2^{2+} cation with a O7−U1−O6 bond angle of 179.8(1)°. The uranium metal center, shown in Figure 5, is equatorially bound to four phosphonoacetate ligands to form an overall pentagonal bipyramidal geometry. Two phosphonoacetate ligands are bound in a monodentate fashion through an oxygen atom of the phosphonate (O3, O4) with an average bond distance of 2.327 Å, whereas one ligand is bound to the uranium metal center through a carboxylate oxygen (O5) with a bond distance of 2.468(2) Å. Additionally, one phosphonoacetate ligand is bound in a bidentate fashion to the uranium metal center through a phosphonate oxygen (O1) and a carboxylate oxygen (O2) at distances of 2.348(2) and

(79) Bond-valence summation confirmed that O19, O24, O25, and O27 are water molecules. A table listing calculated valence unit values can be found in the Supporting Information as SI7.

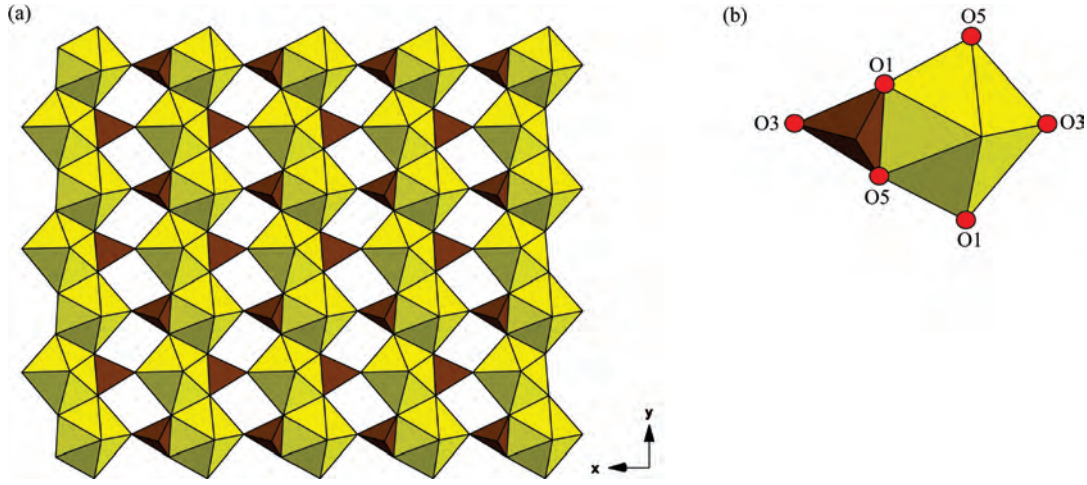

Figure 1. (a) Polyhedral representation of **1** viewed down the [001] direction demonstrating the propagation of edge-shared UO_2^{2+} polyhedra along [010]. Coordination of the phosphonoacetate ligands to the U(VI) metal centers occurs exclusively via the phosphonate oxygens to result in 2D sheets. (b) Illustration showing the local coordination of the U(VI) site. Yellow polyhedra are uranium (VI) atoms in pentagonal bipyramid geometry. Brown polyhedra represent the phosphorus atoms of the phosphonoacetate ligand.

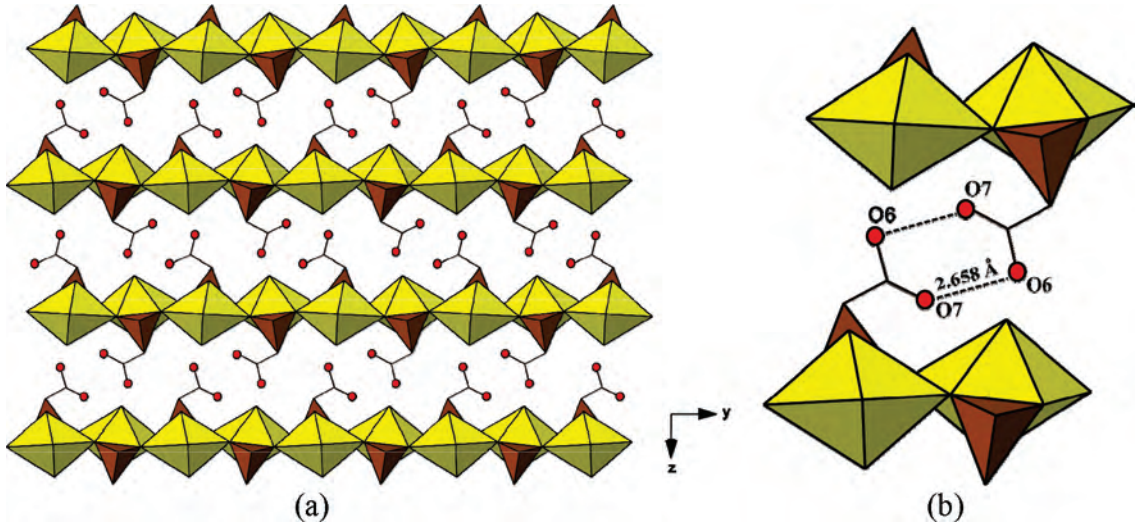

Figure 2. (a) View of **1** down the [100] direction illustrating the stacking of the uranium phosphonate sheets along [001]. As can be seen here, the unbound carboxylate units protrude into the interlayer where hydrogen bonding between these moieties results in additional stabilization of the structure (b) Illustration of head-to-head O(6)−H and O(7) hydrogen bonding network that constitutes the interlayer.

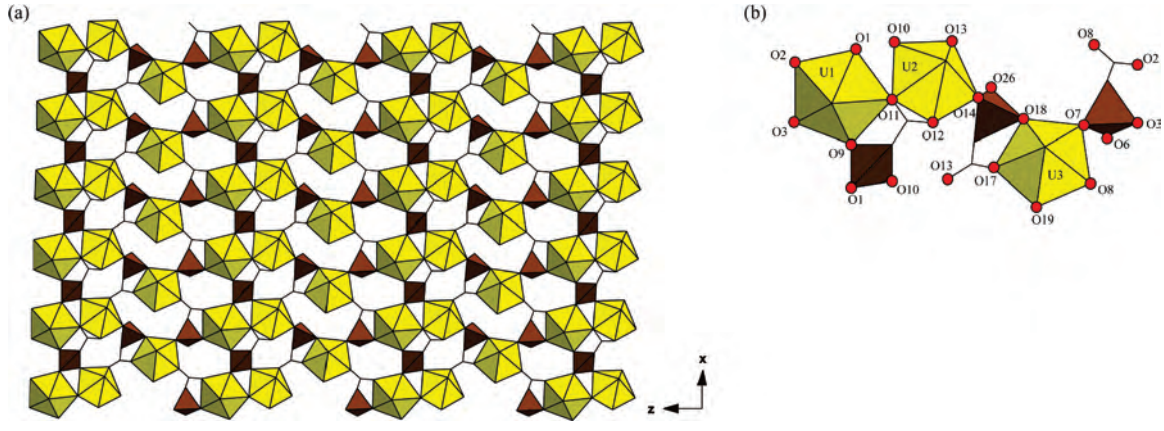

Figure 3. Polyhedral representations of **2** (a) viewed down the [010] direction illustrating the topology of the sheet and (b) demonstrating the coordination environment of each UO_2^{2+} cation. Yellow polyhedra are U(VI) atoms in pentagonal bipyramid geometry. Brown polyhedra and black lines represent the phosphorus and carbon atoms of the phosphonoacetate ligand.

2.458(2) Å, respectively. As depicted in Figure 5, the uranium monomers are linked via the phosphonoacetate ligands along the [100] and the [010] directions to form 2D sheets. Figure 6 illustrates the stacking of the sheets along the [001] direction with solvent water (omitted for clarity) and ammonium molecules residing in the interlayer.

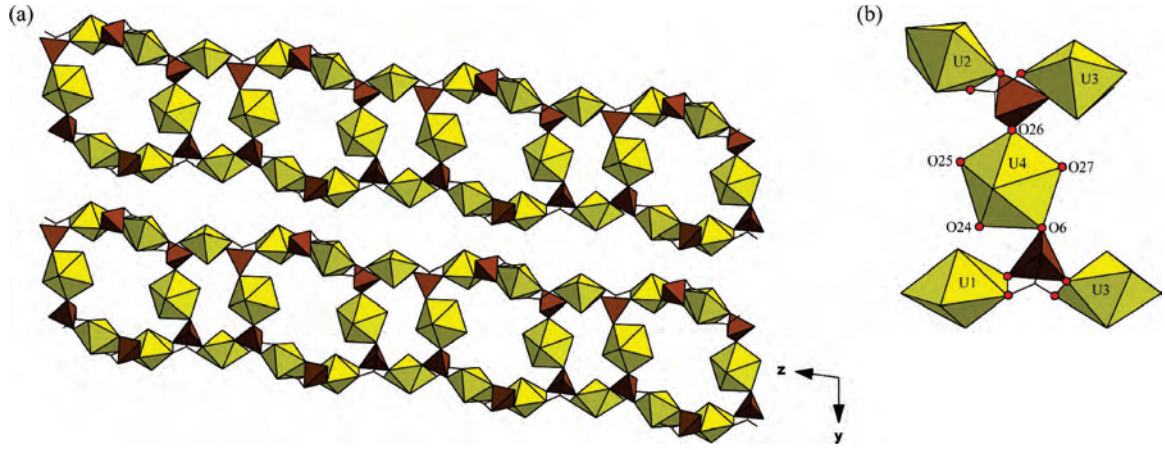

Figure 4. (a) Illustration of **2** showing the tunnels that extend infinitely along [100]. Two layers are tethered via discrete $U(4)O_2^{2+}$ pentagonal bipyramids to result in thick slabs that stack along [010]. (b) Polyhedral representation of **2** demonstrating the local coordination environment of $U(4)O_2^{2+}$. Solvent water molecules have been omitted for clarity.

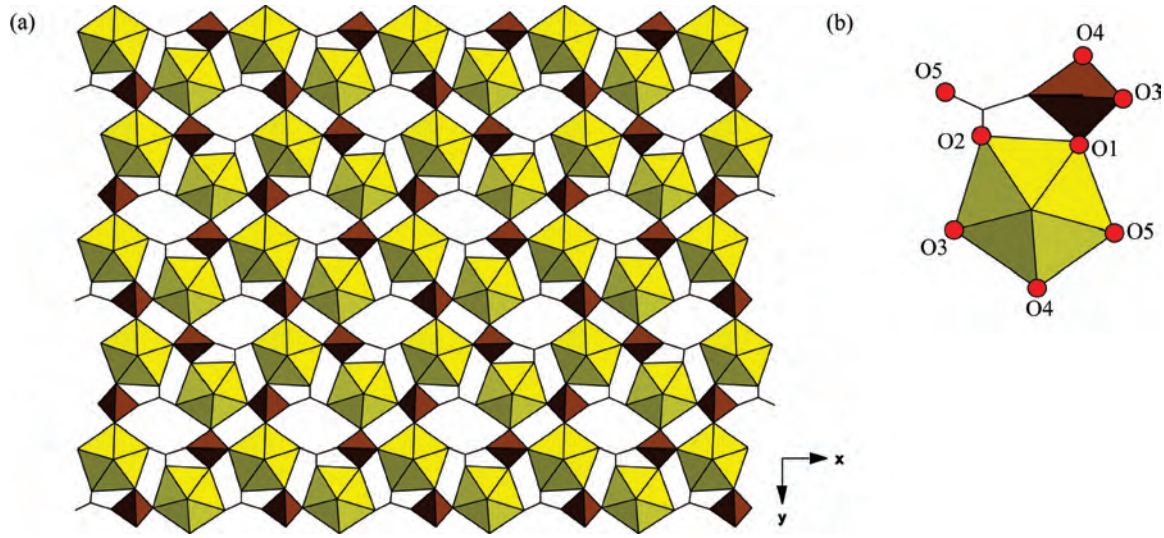

Figure 5. (a) Polyhedral representation of **3** viewed down the [001] direction. The compound consists of U(VI) pentagonal bipyramids linked by phosphonoacetate molecules to form a 2D network. (b) The local coordination environment of the UO_2^{2+} cation.

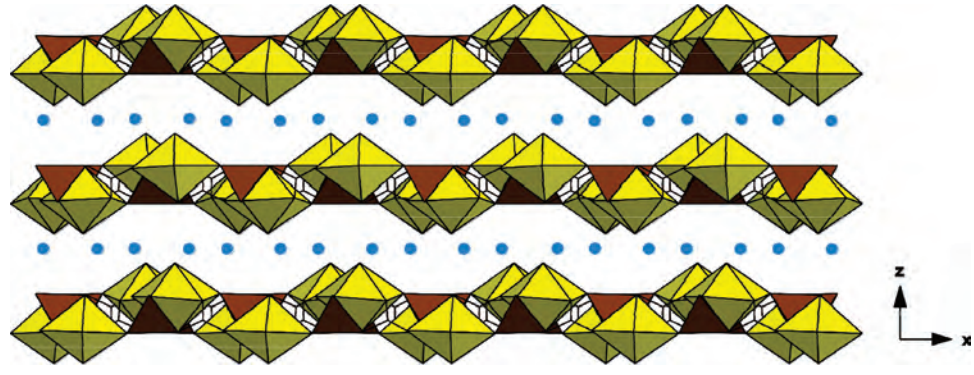

Figure 6. View of **3** viewed down [010] showing the stacking of uranium phosphonoacetate layers along [001]. The anionic sheets are charge balanced by ammonium cations found in the interlayer. Water molecules have been omitted for clarity.

The structure of **4**, $(UO_2)_3(O_3PCH(CH_3)CO_2)_2(O_3PCH(CH_3)CO_2H)\cdot 2NH_4\cdot H_2O$, contains two crystallographically distinct UO_2^{2+} metal centers. The first UO_2^{2+} is constructed from a central uranium (U1) bound to two axial oxygen atoms (O4 and O8) at distances of 1.763(5) and 1.773(5) Å respectively with a O4−U1−O8 angle of 178.2(3)°. As shown in Figure 7, U1 is equatorially coordinated to five oxygen atoms from three 2-phosphonopropionate ligands to form pentagonal bipyramid geometry. Two symmetry-equivalent 2-phosphonopropionate units are bound in a bidentate fashion through a phosphonate and a carboxylate oxygen (O11 and O1 respectively), whereas the third molecule is coordinated through a single phosphonate oxygen (O3) of an additional acid molecule. Similarly, the second

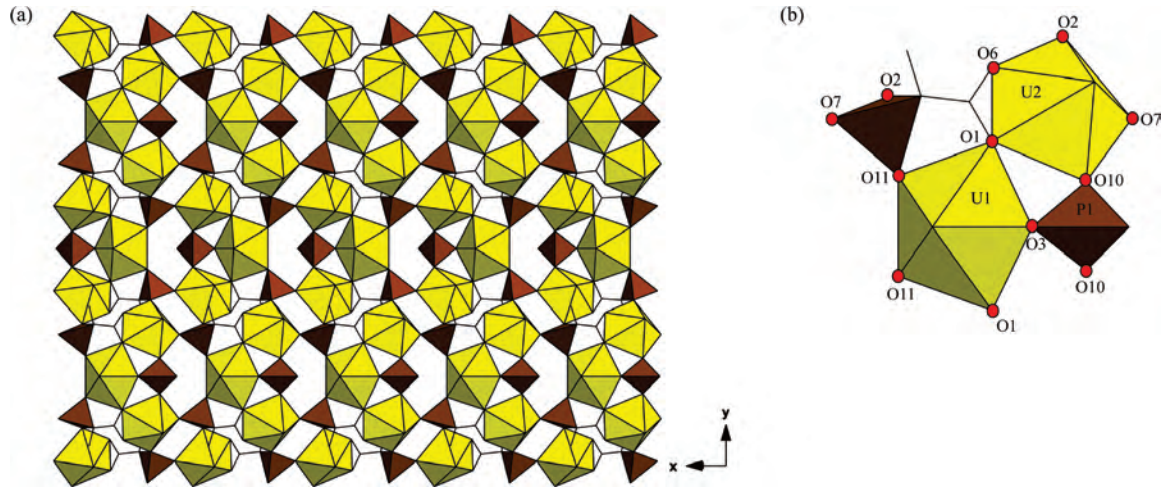

Figure 7. (a) Polyhedral illustration of **4** viewed down the [001] direction demonstrating the topology of the 2D sheets. (b) The phosphonopropionate units exhibit two distinct binding modes. One coordinates to four UO_2^{2+} centers through carboxylate and phosphonate oxygens, whereas another coordinates to three U(VI) polyhedra solely through phosphonate oxygens. Disordered $-CH_3$ and $-CO_2$ functional groups that reside on the P(1) phosphonopropionate ligand have been omitted for clarity.

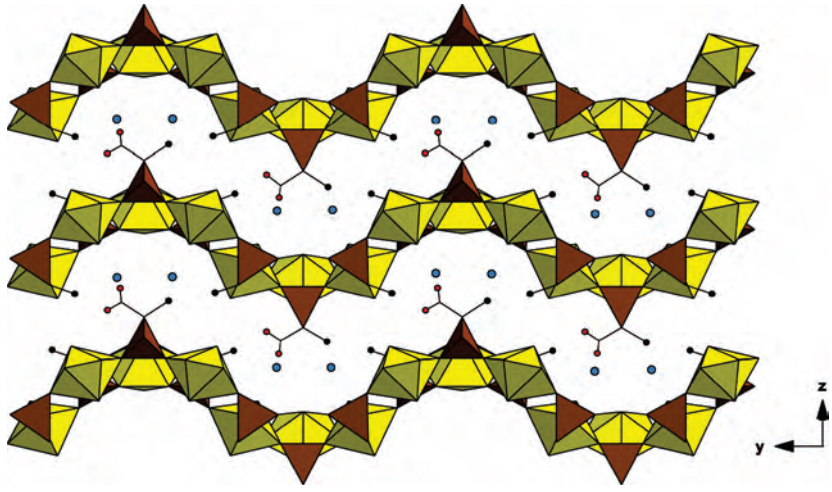

Figure 8. View of **4** down [100] illustrating the stacking of the layers. The uncoordinated carboxylates as well as the methyl groups protrude into the interlayer. Disorder of the unbound carboxylate/methyl group across the mirror plane is not shown.

UO_2^{2+} is formed via coordination of U2 to two axial oxygens (O5 and O9) at distances of 1.760(4) and 1.771(4) Å with an O5−U2−O9 angle of 178.6(1)°. The pentagonal bipyramid geometry of U2 is completed via coordination of three phosphonate oxygens (O2, O7, O10) from three monodentate ligands and two carboxylate oxygens (O1, O6) from a bidentate phosphonopropionate molecule. The structure contains $(UO_2)_3(O)_{13}$ trimers (consisting of a central $U(1)O_2^{2+}$ that point shares with two symmetry-equivalent $U(2)O_2^{2+}$ metal centers via O1) that propagate down the [100] direction through phosphonate linkages. Application of the 2_1 screw axis along [010] gives rise to the 2D sheets (Figure 7). The unbound carboxylate from one phosphonopropionate unit and the methyl groups of both acid molecules extend into the interlayer and as a consequence significant undulation within the layers occurs as illustrated in Figure 8. Although not shown, these moieties are disordered across a mirror plane. Additionally, ammonium cations reside in the interlayer and act to charge balance the anionic sheets.

Thermogravimetric Analysis

The weight loss for **1** began at 400 °C and occurred in a single step to 480 °C. The total weight loss over this range was 13%, which corresponds to the decomposition of the phosphonoacetate unit. The TGA curve for **2** exhibits three weight loss steps. The first step took place between 35 and 75 °C with an initial weight loss of ∼3%, consistent with the loss of three lattice water molecules. A second weight loss occurred between 100 and 300 °C and can be attributed to the loss of the four bound water molecules. Several TGA measurements were carried out, and it appeared that the total weight loss over the temperature range 30 to 300 °C was consistently between 8 and 9% with an initial 3% loss occurring at ∼35 °C. The third step occurred between 325 and 425 °C and is attributed to the decomposition of the phosphonoacetate ligand. The weight loss for **3** occurred in two steps. Loss of lattice water from the structure began just after 150 °C and was complete by 300 °C. Subsequent loss of the ammonium cation and decomposition of the organic

Table 4. Assignment of the Infrared Spectra for **1**−**4**

compound	wavenumber (cm^{-1})/ intensity[a]	assignment
2, **3**, **4**	3512, 3584, 3542 (s)	O−H stretch in U-coord H_2O
2, **3**, **4**	3201 (br), 3367, 3404 (br) 3251 (s)	O−H in lattice water
1, **4**	3011; 3063	O−H in COOH
1, **3**, **4**	2970, 2922; 2977, 2868; 2958, 2893	$-CH_2$
1, **4**	1702(s), 1742(s)	C═O unbound
2, **4**	1636 (w); 1639 (w)	H_2O bending
2, **3**, **4**	1542; 1575 (doublet); 1557	O−C−O antisymm stretch
3, **4**	1435; 1418	NH_4^+
2, **3**, **4**	1380; 1402 (doublet); 1376	O−C−O symm stretch
1−**4**	1210−995 (multiple, s)	*P*═O and P−O asym and sym stretching
1−**4**	957; 958, 922; 945, 917; 986, 934 (vs)	U═O antisymm stretch
1−**4**	862; 828; 829, 812; 851, 820(w)	U═O symm
1−**4**	600−500 (multiple, s)	O−P−O bending

[a] vs = very strong; s = strong; m = medium; w = weak; br = broad.

occurred and was complete by ∼530 °C. The total weight loss for **4** was nearly 14.5%. An initial weight loss of 3% occurred between 150 and 310 °C, consistent with the loss of one lattice water and one ammonium molecule. The second loss occurred immediately thereafter with an additional weight loss of ∼11%, which can be attributed to the loss of the additional ammonium cation as well as decomposition of the phosphonopropionate molecule. Decomposition was complete by 520 °C. The TGA curves for **1**−**4** are consistent with decomposition of the materials to multiple uranyl phosphate phases that likely include $UO_2H_2P_2O_7$, $(UO_2)_2(P_2O_7)$, and $(UO_2)_3(PO_4)_2$. Powder X-ray diffraction data and IR spectra of the resulting products support this finding. The IR spectra contain peaks at average values of 2341 and ∼1000 cm^{-1} that are attributed to P−H (str)[80] and P−O (very broad) stretches, respectively.[68] Decomposition of these materials to phosphate containing phases is consistent with the thermogravimetric behavior of other metal phosphonates.[33,81,82] All TGA plots, powder diffraction data and IR spectra are available in the Supporting Information (Figures SI10−17).

IR Spectra. For **1**−**4**, the high wavenumber region of the IR spectra are dominated by the O−H and C−H stretches. For **1** and **4**, the ν(C═O) of the unbound carboxylate moieties are observed at ∼1700 cm^{-1}, whereas the ν(C═O) of the bound carboxylate groups in the IR spectra of **2**−**4** are observed between 1550 and 1400 cm^{-1}. The low-energy region exhibits peaks indicative of the phosphonate, P−O, and uranyl stretches. These results have been summarized and peak assignments are given in Table 4. The observed stretches are at expected values as compared to those reported for uranium phosphates, uranium organophosphonates, and/or structures containing phosphonocarboxylate ligands.[23,81–84]

Fluorescence Studies. The emission spectra for **2** and **3** exhibited the characteristic vibronic structure of the UO_2^{2+} cation.[54,76] The five characteristic peaks ranged from 475 to 600 nm. Alternatively, **1** and **4** exhibited diminished emission. **1** and **4** are structurally similar in that they each consist of unbound carboxylate groups that extend into the interlayer. It is possible that this structural feature provides an alternative nonradiative decay pathway that results in the lack of emission observed in these materials. The emission spectra for **1**−**4** are available in the Supporting Information (Figures SI 18−21).

Discussion

The solid-state structures herein illustrate the rich structural diversity that exists within uranyl-containing inorganic−organic hybrid architectures. With the exception of **1**, the sheet topologies observed here have not been previously reported within U(VI) phosphate or phosphonate chemistry. In comparison to uranium(VI) phosphates, uranyl carboxyphosphonates are constructed with more flexible building units (i.e., linker), and incorporation of the acetate functionality gives rise to a variety of structural entities not available within strictly phosphate structural chemistry.

As mentioned previously, researchers have a variety of synthetic tools to target or design new structure types. Recently, in situ ligand formation within hydro(solvo)thermal systems has been recognized as a powerful synthetic strategy.[62] Fueled largely by serendipitous discovery and less by intentional design, these reactions have been shown to simplify syntheses, offer greener routes to known compounds, promote single-crystal growth, and in some cases even provide a pathway to materials inaccessible otherwise.[64] Within phosphonate chemistry, in situ hydrolysis reactions have been used for the purpose of (1) removing the need to synthesize the acid form of the ligand[85] and (2) obtaining crystals of suitable size for structural characterization.[35,81,86] With these principles in mind and encouraged by recent examples of in situ ligand transformations in our own laboratory, we explored the hydrothermal reactions of uranium oxynitrate with both the acid ($H_2O_3PCH_2CO_2H$) and the trialkylester ($Et_2O_3PCH_2CO_2Et$) forms of the phosphonoacetate ligand shown in Scheme 2. These studies resulted in **1** and **2**, respectively. Subsequent reactions that accounted for the hydrolysis products generated in situ (i.e., 3 equiv of ethanol) but were otherwise identical to that previously yielding **1** were investigated. Addition of the ethanol resulted in **2** and these results are depicted in Figure 9. These findings highlight an important aspect and challenge with regard to hydrothermal syntheses. In this

(80) Nakamoto, K. *Infrared and Raman Spectra of Inorganic and Coordination Compounds Part B: Applications in Coordination, Organometallic, and BioInorg. Chem.*, 5th ed.; John Wiley & Sons, Inc: New York, 1997.
(81) Hix, G. B.; Kariuki, B. M.; Kitchin, S.; Tremayne, M. *Inorg. Chem.* **2001**, *40*, 1477–1481.
(82) Fu, R.; Xiang, S.; Zhang, H.; Zhang, J.; Xu, X. *Cryst. Growth Des.* **2005**, *5*, 1795–1799.
(83) Sun, Z.-G.; Dong, D.-P.; Li, J.; Cui, L.-Y.; Zhu, Y.-Y.; Zhang, J.; Zhao, Y.; You, W.-S.; Zhu, Z.-M. *J. Coord. Chem.* **2007**, *60*, 2541–2547.
(84) *Uranium: Mineralogy, Geochemistry and the Environment*; Burns, P. C., Finch, R., Eds.; Mineralogical Society of America: WA, 1999; Vol. 38.
(85) Jaffrès, P.-A.; Villemin, D.; Caignaert, V. *Chem. Commun.* **1999**, 1997.
(86) Zhang, X.-M. *Eur. J. Inorg. Chem.* **2004**, *54*, 4–548.

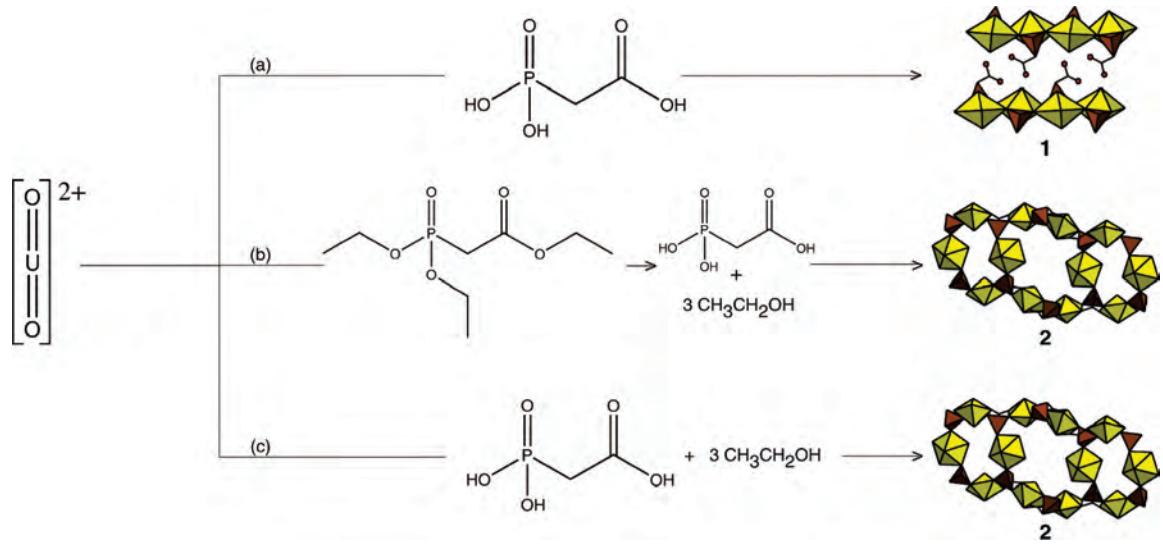

Figure 9. Illustration depicting the compounds obtained from the reaction of UO_2^{2+} with (a) phosphonoacetic acid, (b) triethylphosphonoacetate, and (c) the hydrolysis products of the trialkylphosphonate ligand.

case, the formation of **2** was favored over **1** upon the addition of ethanol, a spectator species, to the reaction solution. In terms of product assembly and formation, in this case, we speculate that EtOH may (1) disrupt/change the intermolecular interactions (i.e., hydrogen-bonding) that support the construction and stabilization of **1**; (2) modify the solution kinetics so as to favor the nucleation and growth of **2**; or (3) alter the solubility and hence favor the precipitation of a particular phase. Incorporation of second organic species therefore must be considered.

Consistent with these observations, Hou et al. similarly described instances where amines were found to act as additives presumably necessary for product synthesis.[35] They explored the utility of organic amines 4,4′-bipyridine, *N*,*N*′dimethylpiperazine, *N*-ethylpiperazine, and piperazine in the preparation of a series of transition-metal phosphonoacetates. Synthetically and structurally, the amine acted in a variety of roles. Interestingly, in four of the materials synthesized, the amines were absent from the solid-state structure. In these instances, the organic was an otherwise spectator species or alternatively may have played a role in the redox chemistry necessary for the formation of an Fe(III) ppa phase. That is to say that the amine was not present in the crystalline product and did not contribute to the topology in an observable manner. The remaining three structures contained the amine in the crystalline reaction product as either a coordinating species or a template.

Most generally speaking, the addition of a template to a synthesis may provide a noncoordinating species around which an inorganic framework can form. In this sense, a template can act in one of the following ways: as a structure directing agent, as a space filling species, or as a charge-balancing counterion.[87] In the capacity of the latter, the addition of NH_4^+ to UO_2^{2+}/ppa or 2-pp hydrothermal reactions was investigated. In the structures of **3** and **4**, ammonium cations charge balance the anionic sheets. Moreover, NH_4^+ may be considered to direct the formation of **3** (and perhaps **4**) by disrupting, or adjusting, the hydrogen bonding networks found in **1** and **2**. Reactions similar to that reported for **4**, without NH_4^+, were also studied. Although powder X-ray diffraction data confirmed the presence of a different phase, crystals suitable for structural characterization by single-crystal X-ray diffraction could not be isolated, and thus the NH_4^+ directed synthesis of UO_2^{2+}/2-pp phases cannot likewise be discussed.

In the absence of information obtained in situ, examination of crystalline, solid-state materials has historically provided valuable insight into product formation and stabilization. Review of structural features has thus allowed us to classify materials based on similarities and differences present within a variety of architectures. As such, the building units, metal−ligand binding modes, intermolecular interactions, and the implications of such features on the topology and overall dimensionality of **1**−**4** have been considered and will be discussed.

The compounds presented here are all constructed from the uranyl (UO_2^{2+}) cation in pentagonal bipyramid geometry. Additionally, **1**−**3** all similarly consist of phosphonoacetate (ppa) units. Despite the presence of similar building blocks, the topologies of these materials vary quite significantly. This is most seemingly a result of the various metal−ligand coordination modes that uniquely contribute to the assembly of each material. Whereas the structure of **4** consists of 2-phosphonopropionate (2-pp) molecules, addition of the methyl group at C2 (in comparison to ppa) does not alter alkane chain length or functionality but has basic implications with regard to steric considerations rather than coordination modes. For example, as illustrated in Figure 8, the uncoordinated carboxylate as well as the methyl groups of **4** extend into the interlayer and have considerable ramifications (undulation within the layers) on the overall structure. Both carboxyphosphonate linkers used in this study present the same five feasible metal binding modes as illustrated in Figure 10. Collectively, each of these modes has been

(87) Davis, M. E.; Lobo, R. F. *Chem. Mater.* **1992**, *4*, 756–768.

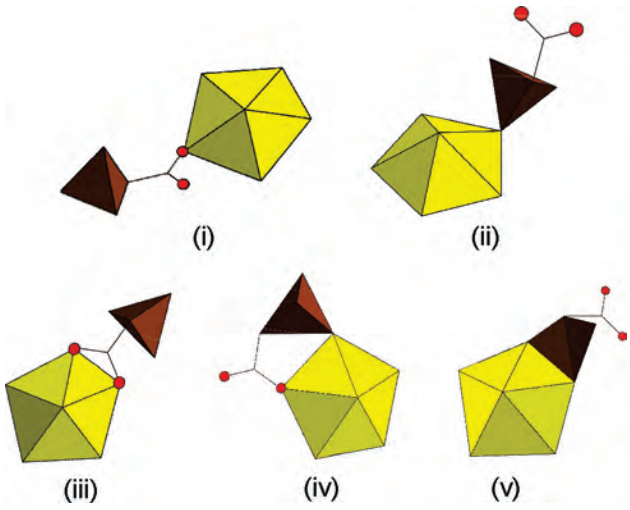

Figure 10. Illustration of the various metal-to-ligand binding modes found within **1**−**4**. The ligand exhibits monodentate (i, ii) and bidentate (iii–v) linkages.

observed with the most common linkage occurring through a phosphonate oxygen (10-ii) as observed in **1**−**4**. As seen in **2** and **3**, ppa may alternatively bind to UO_2^{2+} in a monodentate manner via (10-i) a carboxylate oxygen. The ligand may also coordinate to the uranyl site in a bidentate fashion by (10-iii) two carboxylate oxygens (**2** and **4**), (10-iv) a phosphonate and carboxylate oxygen (**2**, **3**, and **4**) or (10-v) two phosphonate oxygens as observed exclusively in **1**.

In a search of the Cambridge Structural Database (using *Conquest* version 5.29, 2008 release),[88,89] approximately 30 structures were found that consisted of group II, transition, or lanthanide metal cations coordinated to phosphonoacetate or 2-phosphonopropionate molecules. Of those, 20 were reported wherein the chelation of the $-PO_3$ and $-CO_2$ oxygen atoms to form stable six-membered rings (10-iv)[35] was observed. Conversely, and though relatively common in M^{2+}/Ln^{3+} mono- and diphosphonate crystal chemistry,[23,47] observation of mode (10-v) within ppa bearing architectures, specifically, has been limited to that reported by Slepokura et al. for $[Ca(C_2H_4O_5P)2]_n$.[90] Furthermore, and to the best our knowledge, the bidentate linkage of a single ppa to UO_2^{2+} via carboxylate oxygen atoms (10-iii), as seen in **2**, represents the first occurrence within a ppa-containing material. The metal phosphonocarboxylates reported thus far have most commonly included hard lewis acids, and therefore the absence of (10-iii) in metal ppa containing materials may be related to the affinity of group II, transition metal (II), or lanthanide(III) metal cations for harder ($-PO_3^-$) functional groups. U(VI) is likewise a hard acid; however, the nominally terminal nature of the UO_2^{2+} oxygen atoms predispose the cation to coordination almost exclusively in the equatorial plane. The size and coordination requirements of the uranyl cation thus lend it to unique coordination modes. In this regard, heterofunctional phosphonocarboxylates are also attractive candidates for bimetallic inorganic−organic materials synthesis wherein metal binding preferences could be investigated and potentially utilized to construct novel architectures. Whereas chelation of U(VI) via the carboxylate oxygen atoms (10-iii) has been rare in ppa structures, incorporation of ligands structurally related to ppa (differ only in alkane chain length) such as 3-phosphonopropionate[91] have also yielded compounds constructed from (10-iii). As reported for other metal phosphonoacetates and also this work, formation of stable six-atom rings (i.e., P−O−U−O−C−C) is common. Linker structure and steric constraints are also important factors in inorganic−organic network assembly.

The carboxyphosphonate units can also be described in terms of linking U(VI) metal centers into extended networks. These building units likewise have a considerable effect on the resulting topology. **1**−**4** collectively exhibit seven coordination modes. As illustrated in Figure 11, the ppa and 2-pp units connect either three (a−c) or four (d−g) uranium(VI) polyhedra. Whereas modes d−g are noticeably similar, slight distinctions arise from the orientation of the phosphonate group with respect to the acetate group and additionally influence the topologies of **1**−**4**. This relation may be described in terms of O−P−C−C and P−C−C−O torsion angles listed in Table 5. The overall structures of the phosphono groups in **1**−**4** are similar to that previously reported in phosphonoacetic acid[92] and $[Ca(C_2H_4O_5P)_2]$,[90] with the carboxylic carbon atom lying nearly trans to one of the phosphonate oxygen atoms and virtually gauche with respect to the other phosphonate oxygen atoms. The values for the P−C−C−O torsion angles for **1**−**4**, however, show much variability, ranging from approximately (±)30 to (±)170° and thus account for some of the structural diversity viewed here. As seen in Table 5, **1** and **3** have similar P−C−C−O torsion angles with values of [−156.36, 23.37] and [158.45, −28.34], respectively. Interestingly, the structure of **1** consists of uncoordinated carboxylate groups that protrude into the interlayer to form a hydrogen bonding network, whereas **3** is constructed from phosphonoacetate units that coordinate within the layer to form anionic sheets. Ammonium cations reside in the interlayer, and it is likely that their presence governs the structural differences observed here.

Another exciting structural feature of these materials is the variety of the U(VI) polyhedral units. Within purely inorganic and inorganic−organic UO_2^{2+} materials, structures built from monomers, dimers, or chains of edge-sharing uranyl polyhedra are quite common.[77,78] Likewise, and specifically within uranyl phosphate or phosphonate containing architectures, extended networks are frequently constructed from edge sharing polyhedra or alternatively uranyl monomers linked via PO_4^{3-} or $R-PO_3$ moieties. Thus, the observation of chains of edge-sharing uranyl polyhedra in **1** and the UO_2^{2+} monomers linked via phosphonate tetrahedra

(88) Allen, F. H. *Acta Crystallogr.* **2002**, *B58*, 380–389.
(89) Bruno, I. J.; Cole, J. C.; Edgington, P. R.; Kessler, M.; Macrae, C. F.; McCabe, P.; Pearson, J.; Taylor, R. *Acta Crystallogr.* **2002**, *B58*, 389–397.
(90) Slepokura, K.; Lis, T. *Acta Crystallogr., Sect. C* **2003**, *59*, m76–m78.
(91) Zhang, X. M.; Fang, R. Q.; Wu, H. S. *Cryst. Growth Des.* **2005**, *5*, 1335–1337.
(92) Lis, T. *Acta Crystallogr., Sect. C* **1997**, *53*, 28–42.

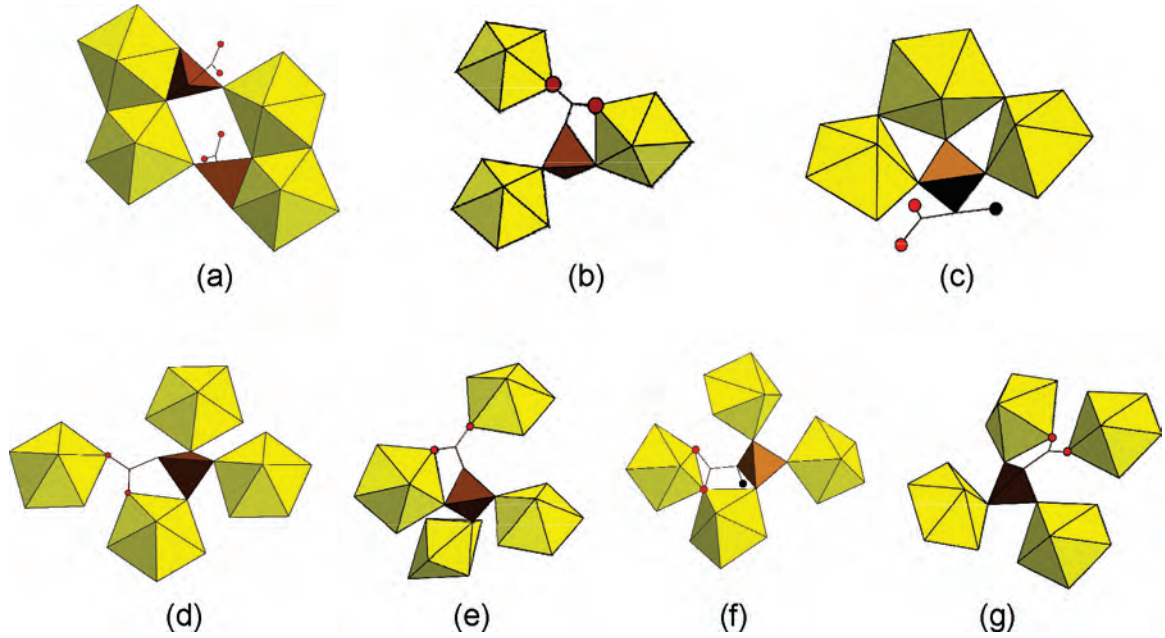

Figure 11. Polyhedral representation of the building units found within **1**−**4** illustrating the various modes by which the phosphonocarboxylate ligands link metal centers. Modes a−c contain protonated oxygen atoms that do not coordinate to the uranium metal center. Both a (found in **1**) and c (found in **4**) have protonated carboxylate oxygens, whereas (b) (found in **2**) contains a protonated phosphonate oxygen. Modes d−g each consist of a coordinatively saturated phosphonocarboxylate unit that acts to link four UO_2^{2+} cations. Note: illustrations a,b, d, e, and g are constructed from ppa molecules, whereas c and f depict the 2-pp ligand.

Table 5. Selected Torsion Angles (Degrees) for **1**−**4**

1					
O(6)−C(2)−C(1)−P(1)		−156.36	O(1)−P(1)−C(1)−C(2)		−66.88
O(7)−C(2)−C(1)−P(1)		23.37	O(5)−P(1)−C(1)−C(2)		−177.13
O(3)−P(1)−C(1)−C(2)		58.14			
2					
O(2)−C(2)−C(1)−P(1)	62.37	O(11)−C(4)−C(3)−P(2)	−73.72	O(13)−C(6)−C(5)−P(3)	169.69
O(8)−C(2)−C(1)−P(1)	−119.25	O(12)−C(4)−C(3)−P(2)	101.18	O(17)−C(6)−C(5)−P(3)	−37.57
O(3)−P(1)−C(1)−C(2)	−49.75	O(1)−P(2)−C(3)−C(4)	170.28	O(14)−P(3)−C(5)−C(6)	−55.85
O(6)−P(1)−C(1)−C(2)	−170.53	O(9)−P(2)−C(3)−C(4)	48.71	O(18)−P(3)−C(5)−C(6)	62.66
O(7)−P(1)−C(1)−C(2)	69.88	O(10)−P(2)−C(3)−C(4)	−68.42	O(26)−P(3)−C(5)−C(6)	−178.03
3					
O(2)−C(2)−C(1)−P(1)		−28.54	O(1)−P(1)−C(1)−C(2)		40.26
O(2)−C(2)−C(1)−P(1)		158.45	O(3)−P(1)−C(1)−C(2)		160.59
			O(4)−P(1)−C(1)−C(2)		−79.06
4					
O(1)−C(1)−C(2)−P(2)		−73.09	O(40)−C(5)−C(4)−P(1)		93.53
O(6)−C(1)−C(2)−P(2)		104.79	O(41)−C(5)−C(4)−P(1)		−91.37
O(2)−P(2)−C(2)−C(1)		−59.07	O(2)−P(2)−C(2)−C(1)		58.15
O(7)−P(2)−C(2)−C(1)		179.00	O(7)−P(2)−C(2)−C(1)		175.10
O(11)−P(2)−C(2)−C(1)		59.31	O(11)−P(2)−C(2)−C(1)		−63.37

in **3** is not surprising. In contrast, the point sharing dimers and trimers viewed in **2** and **4**, respectively, are less common. Point-sharing dimers have been reported for few UO_2^{2+}-containing architectures including $(NH_4)[(UO_2)_2(OH)(C_2O_4)_2]\cdot 2H_2O$,[93] whereas, to the best of our knowledge, there have been no previous accounts of point sharing trimers such as those observed in **4**.

In addition to the metal−ligand binding modes that constitute the 2D sheets in **1**−**4**, alternative modes of connectivity are observed. Most noticeably, the structure of **1** is additionally stabilized by a moderately strong and extensive O−H···O hydrogen bonding network. The hydrogen bonds viewed in **1** are formed by the carboxylate moieties that reside in the interlayer wherein the carboxylic groups from adjacent layers are connected to each other by the O−H···O interactions. Such hydrogen bonding schemes have similarly been observed within metal diphosphonate[15] and phosphonocarboxylate materials.[19,90] Alternatively, the structure can be stabilized by C−H···O interactions such as those found in **4** or via N−H···O as seen in **3**.

In conclusion, four new U(VI) carboxyphosphonates have been synthesized by hydrothermal reactions and structurally characterized. Several factors, including in situ ligand formation, spectator species, incorporation of charge-balancing countercations, building units, metal−ligand binding modes, and torsion angles contribute to the assembly of these

(93) Cahill, C. L.; Borkowski, L. A. In *Structural Chemistry of Inorganic Actinide Compounds*; Krivovichev, S. V., Burns, P. C., Tananaev, I. G., Eds.; Elsevier: Amsterdam, The Netherlands, 2007; p 419.

architectures and give rise to rich structural variation. Hydrogen bonding networks are also shown to play a critical role in the formation and stabilization of the various structure types. The fluorescent properties and thermal behavior of these materials have been explored and the results are consistent with those previously observed for U(VI) coordination polymers and metal carboxyphosphonates, respectively.

Acknowledgment. This work was supported by 1) the National Science Foundation (DMR-0348982 and DMR-0419754), 2) the Chemical Sciences, Geosciences and Biosciences Division, Office of Basic Energy Sciences, Office of Science, Heavy Elements Program, U.S. Department of Energy, under grant DE-FG02-05ER15736 at GWU, and 3) the ARCS (Achievement Reward for College Scientists) Foundation, Metropolitan Washington tuition reward to K.E.K. The authors are indebted to Victor G. Young for helpful discussions regarding the refinement of structure **4**.

Supporting Information Available: This material is available free of charge via the Internet at http://pubs.acs.org.

IC800683M